Catalysis Science & Technology

Accepted Manuscript

ROYAL SOCIETY OF CHEMISTRY

www.rsc.org/catalysis

The conversion of levulinic acid into γ-valerolactone using Cu-ZrO_2 catalysts

Daniel R. Jones,[a] Sarwat Iqbal,[a] Satoshi Ishikawa,[a,b] Christian Reece,[a] Liam Thomas,[a] Peter J. Miedziak,[a] David J. Morgan,[a] Jennifer K. Edwards,[a] Jonathon K. Bartley,[a] David J. Willock,[a] Graham J. Hutchings [a,*]

*hutch@cardiff.ac.uk

[a] *Cardiff Catalysis Institute, Main Building, Park Place, Cardiff, CF24 3AT*

[b] *Catalysis Research Centre, Hokkaido University, N-21, W-10, Sapporo, 001-0021, Japan*

Abstract

A series of Cu-ZrO_2 catalysts prepared by a co-precipitation method were studied for the hydrogenation of levulinic acid to give γ-valerolactone (GVL). The effect of a range of catalyst preparation parameters, namely molar Cu/Zr ratio, calcination temperature and the ageing time of the precipitates, were systematically investigated. The molar Cu/Zr ratio was found to have a strong influence on the BET surface area of the material leading to a high activity for catalysts prepared with a Cu/Zr molar ratio of unity. Using this molar ratio the calcination temperature was varied from 300 °C to 800 °C, the material calcined at 400 °C showed the highest activity. Increasing the ageing time used in the catalyst preparation identified 6 h as the optimum to achieve the highest activity for LA conversion. Based on characterisation of all materials we conclude that the active Cu species is present in only low concentration suggesting that it should be possible to produce a catalyst of high activity with much lower Cu content.

Key words: Cu, ZrO_2, levulinic acid, GVL, hydrogenation

Introduction

Biomass is an increasingly important alternative to fossil based sources of fuels and chemicals which will require efficient processing technologies in order to meet future energy demands.[1-3] Lignocellulose is an attractive source of biomass since it does not compete with food production. Finding effective ways to utilize lignocellulose is a current challenge leading to an increased research activity in this area in recent years.[4]

The breakdown of lignocellulose into sugars, followed by their consecutive dehydration and hydrogenation to levulinic acid (LA) is well established.[5] LA can be obtained by the acid hydrolysis of hexoses (C_6 sugars), which can be synthesized inexpensively from the decomposition of cellulose.[6, 7] In addition to LA, formic acid (FA) can be coproduced by acid-catalysed conversion of C_6 sugars.[8] Accordingly, the processing of LA has been identified as one of the most important challenges for increasing the effective use of biomass in the chemical and fuel sectors.[3, 9, 10] LA is an interesting starting material for the production of many useful C_5-based compounds such as γ-valerolactone (GVL),[11] 2-methyltetrahydrofuran (MTHF),[12] and a range of other derivatives.[13] GVL has tremendous potential as a biofuel, with combustion properties comparable to ethanol when blended with gasoline.[14-17] It is also useful industrially as a solvent for insecticides and adhesives, it has extensive uses as a cutting oil, brake fluid and as a coupling agent in dye baths.[12] There is a growing interest in the production of GVL under green reaction conditions. Recently, Dumesic *et al.* reported an integrated process for the production of liquid alkenes from GVL and suggested an inexpensive method to produce GVL from biomass.[18] A number of catalysts for the conversion of LA to GVL have been reported in the literature.[13, 19-23] In general the catalytic systems for GVL synthesis from LA consist of noble metal catalysts (Ru, Au, Pt, Pd) and non-noble metal catalytic systems (Cu, Ni). Ru/C is, by far, the most-reported catalyst for this reaction[24] and has shown outstanding performance in the aqueous phase at mild temperature and pressure (130 ^{o}C, 12 bar H_2). Ruthenium based catalysts are prevalent in the open literature as active catalysts for LA and other liquid phase hydrogenation reactions.[7, 24-31] However, as Ru is a precious metal it is relatively expensive, therefore its wide scale use is difficult to envisage. This makes a push towards utilising catalysts using cheaper more abundant chemical elements desirable.

Cu is one of the most abundant metals that can be used for hydrogenation as an alternative to Ru. Various Cu based catalysts have been reported for the hydrogenation of

levulinic acid.[17, 32, 33] Yan *et al.* [34] have demonstrated Cu–Cr and Cr free Cu-Fe catalysts for efficient synthesis of GVL. Cao *et al.*[35] established that Cu based catalysts can be used for the direct conversion of carbohydrate biomass into GVL without using a H_2 source. Silva *et al.*[36] observed that molybdenum carbide nanoparticles exhibited higher activity and selectivity towards GVL. The application of zirconia as a catalyst support is promising and has been employed in various industrially important reactions. Hengne *et al.* [22] demonstrated, for the first time, nanocomposites of Cu/ZrO_2 and Cu/Al_2O_3 in the liquid phase hydrogenation of LA and its methyl ester to GVL in water and methanol. Both catalysts showed complete conversion of LA and its ester with >90% selectivity towards GVL. Nanocomposites of Cu/SiO_2 have shown effective catalytic performance for the production of GVL. The use of zirconia supported Cu oxide catalysts is of particular interest due to its mechanical strength and high thermal stability.

In the current study a series of $Cu\text{-}ZrO_2$ catalysts were prepared by a co-precipitation method and evaluated for their activity towards LA hydrogenation into GVL. We have studied the effect of variation of catalyst preparation parameters e.g., Cu/Zr ratio, calcination temperature and ageing time of the precipitates. All of these materials were characterized by inductively coupled plasma atomic emission spectroscopy (ICP), X-ray diffraction (XRD), Brunauer–Emmett–Teller (BET) surface area analysis, and temperature programmed reduction (TPR) so as to obtain insight into the structure activity relationship for the catalysis.

Experimental

Catalyst preparation

$Cu\text{-}ZrO_2$ catalysts were prepared by a co-precipitation method adapted from the work of Hengne and Rode. [22] In a typical synthesis calculated amounts of copper nitrate trihydrate ($Cu(NO_3)_2.3H_2O$, 99.0%, Sigma Aldrich) and zirconyl nitrate ($Zr(NO_3)_2.4H_2O$, Sigma Aldrich, ≥98%) were dissolved in water to form a mixed solution with the required Cu:Zr molar ratio for the target material. To this mixture potassium carbonate (0.2 molar, 99%, Fisher Scientific) was added to raise the pH from 3 to 9. The mixture was then aged for 6 h unless otherwise specified and then filtered under vacuum followed by a washing step with hot distilled water (1L). The resulting precipitates were dried (110 °C, 16 h) and calcined at 400 °C for 4 h in static air unless otherwise stated.

To study the effect of calcination temperature, one batch of catalyst was prepared and the dried material was divided into six portions. These portions were calcined separately at 300, 400, 500, 600, 700, and 800 °C in static air for 4 h.

To study the effect of the ageing time, the precipitates were left in the mother liquor for the specific time intervals of 1, 2, 4, 6, 8, 11, 16, and 24 h followed by drying (100 °C, 16 h) and calcination (400 °C, 4h) in static.

Catalyst testing

Experiments for LA hydrogenation were performed in a 50 ml Parr autoclave, equipped with a Teflon liner. In a typical experiment the desired amount of the catalyst was added to 10 ml of the LA solution (5 wt. % LA/H_2O). The autoclave was closed, purged with nitrogen and then with hydrogen. It was then heated to the desired temperature, pressurized with H_2 (35 barg) and stirred at 1000 rpm. After the desired reaction time (2 h unless otherwise stated) the autoclave was placed in an ice bath. When the temperature reached 10 °C the gases were vented (and analysed if stated) and the autoclave was opened. The liquid was filtered and analysed.

Liquid products were analysed using a GC equipped with CP-Sil 5CB (50 m, 0.32 mm, 5 μm) column and FID detector. Acetonitrile was used as an internal standard. Gases were vented into a gas bag and analysed with a GC equipped with TCD and FID detectors and with a methaniser column. Products in the gas phase usually accounted for less than 0.1 % and therefore gas analysis was not performed for every experiment.

Catalyst Characterization

XRD was performed using a PANalytical X'Pert Pro fitted with an X'Celerator detector and a CuKα X-ray source operated at 40 kV and 40 mA, 2θ = 10-80°. Each sample was scanned from 2θ = 10° to 80° for 30 minutes. The catalysts were ground into fine powder before the analysis. The results obtained were compared with the information in SPDF library for each catalyst.

TPR was carried out using a Thermo 1100 series TPDRO under 75 ml/min 5 % H_2/Ar, 10 °C/min ramp rate. Samples (0.1 g) were pre-treated at 110 °C (heating rate = 20 °C min^{-1}) under Ar for 1 hour prior to reduction in order to clean the surface. Analysis was performed under 10%H_2/Ar (BOC 99.99%, 25 ml min^{-1}) 30-800 °C, 20 °C min^{-1}.

X-ray photoelectron spectroscopy (XPS) was performed using a Kratos Axis Ultra-DLD photoelectron spectrometer, using monochromatic Al kα radiation, operating at 144 W power. High resolution and survey scans were performed at pass energies of 40 and 160 eV respectively. Spectra were calibrated to the C (1s) signal at 284.8 eV, and quantified using CasaXPS v2.3.17, using modified Wagner sensitivity factors supplied by the manufacturer.

Surface areas were determined by multi-point N_2 adsorption at 77 K on a Micromeretics Gemini 2360 according to the Brauner Emmet Teller (BET) method. Prior to the analysis, samples were degassed at 120 °C for 1 h under N_2 flow.

Cu surface area analysis was carried out by N_2O pulse titration using a Quantachrome ChemBET. Catalysts were reduced under a flow of 10%H_2/Ar at 250 ^{0}C (5 ^{0}C min^{-1}, held for 20 min). This was followed by cooling under He. N_2O titration was carried out at 65 ^{0}C.

ICP-AES was carried out using an ICPE-9000 instrument by Shimadzu. 25 mg of catalyst was dissolved in 0.5 mL of HF, diluted with 3 mL of HNO_3 and left at 80 °C overnight. After dissolution of the catalyst the solution was diluted to 50 mL with deionised water. 1 mL of this solution was further diluted to 50 mL with deionised water, which was used for the analysis. The instrument was calibrated using Cu and Zr solutions of 0, 0.1, 0.5, 1.0, 2.0, and 5.0 ppm (diluted from a solution of 1000 ppm). The Cu and Zr wavelengths used for the analysis were 213.60 nm and 339.20 nm respectively.

Results and discussion

Influence of Cu/Zr ratio

To study the effect of Cu/Zr metal ratio, catalysts were prepared by the methodology given in the Experimental section with the molar metal ratios of Cu/Zr = 0.25, 0.50, 0.75, 1.0, 1.25, 1.50 and 2.0. ICP-AES analysis showed that the measured Cu/Zr ratios were in good agreement with the theoretical Cu/Zr ratios from the preparation procedure (Supplementary Information Table S1). These catalysts were evaluated for LA hydrogenation under identical reaction conditions and the resulting GVL yield as a function of Cu/Zr ratio is presented in Figure 1a. All catalysts gave essentially 100 % selectivity to GVL so that the GVL yield is equivalent to LA conversion. Each experiment was repeated at least three times and we consistently found a notably higher GVL yield using Cu/Zr = 1 catalysts than for materials with lower Cu/Zr ratios and a gradual decrease of GVL yield with any further increase in the Cu/Zr ratio. GVL yield normalized against the total surface area (BET) of each catalyst as a function

of Cu/Zr ratio is also presented in Figure 1b. The largest surface area was observed for the Cu/Zr molar ratio of 1 and a steady decline in surface area was apparent with further increase in the metal ratio above this level (Supplementary Information Table S2). The normalised GVL yield is dependent on Cu/Zr ratio within experimental error, indicating that the Cu/Zr = 1 composition leads to material with the highest GVL yield and an optimal surface area for the reaction. This is notable, as the amount of Cu in the materials is increasing with Cu/Zr loading whereas the activity as estimated from the normalised yield is constant, suggesting that most of the Cu used in the high ratio materials is not in a catalytically active state.

XRD patterns for all of the catalysts are presented in Figure 2. Two reflections corresponding to CuO appeared at 2θ values of 36° and 39° (ICDD = 00-041-0254) for catalysts prepared with a Cu/Zr ratio of 1; CuO is also confirmed by XPS with the Cu($2p_{3/2}$) signal at 933.2 eV and associated satellite structure and Cu LMM Auger signals at 933.2 eV (binding energy) and 917.7 eV (kinetic energy) respectively and consistent with CuO (Supplementary information, Figure S1). Both reflections became more prominent with an increase in the ratio of Cu/Zr. Two additional reflections of CuO can also be observed at 2θ values of 49° and 62° (ICDD = 00-041-0254) for Cu/Zr ratios of 1.25 and above. The full width half maximum value of the most intense peak at 35° (hkl = (111)) was used to estimate the CuO particle sizes for these materials using the Scherrer equation (Supplementary Information Table S3). The catalysts with low molar Cu/Zr ratio (Cu/Zr = 0.25, 0.5 and 0.75) do not show any CuO reflections in the XRD because of the presence of metal particles with a size less than 5nm. However, XPS analysis does indicate that copper is present as CuO even at these lower ratios.. These catalysts also showed low total surface areas (Table S2) and a low absolute catalytic activity for GVL production from LA hydrogenation (Figure 1a). Even so, the surface area normalised activity for these materials (Figure 1b) is comparable to the most active catalyst in absolute terms (Cu/Zr = 1). The Cu/Zr = 1 material has the lowest metal ratio at which we observe the formation of a CuO phase by XRD analysis and also has the highest BET surface area of any of the catalysts synthesised.

We expect that the presence of CuO is an important feature of these catalysts since CuO particles in the as-prepared material should be converted into Cu particles during the hydrogenation reaction and become important for the catalytic hydrogenation activity. Accordingly, TPR analysis was carried out on all samples to investigate the reducibility of these catalysts; the TPR profiles obtained are shown in Figure 3. For catalysts prepared with Cu/Zr < 0.75, no reduction signals are seen, although ICP-AES indicated Cu was present in all

materials at close to the as-prepared Cu/Zr ratios (Table S1). Cu/Zr catalysts with a ratio of 0.75 do show a broad reduction signal starting around 170 °C centred at 240 °C. We note that the combination of lower Cu content and low surface area for materials with Cu/Zr ≤ 0.75 would suggest that surface Cu species should be between 4 and 16 % that of the Cu/Zr = 1 samples. For example, with a Cu/Zr ratio of 0.25 we obtain a surface area which is only 15 % that of the Cu/Zr = 1 samples (Table S2), coupling this with the loading fraction leads to an estimate for the exposed surface Cu area for the Cu/Zr = 0.25 samples that is only 4% that of the Cu/Zr = 1 materials and this should be expected to contribute to lower TPR signals. Even so, the absence of CuO reduction features in the TPR of Cu/Zr < 0.75 suggests that Cu in the form of CuO was present only at very low levels on the surface and suggests that much of the Cu content is incorporated into the bulk matrix of the zirconia material where it is difficult to reduce. Figure 1a also shows that catalysts with Cu/Zr < 0.75 gave lower than 20% GVL yields under our experimental conditions although the surface area normalised yields (figure 1b) are still comparable to the optimal Cu/Zr = 1 material.

There is a significant change in the reduction profile with an increase in the amount of metals used in the preparation of the catalysts. For Cu/Zr ≥ 1 two reduction events are observed in the temperature range of 150–225 °C. Multiple steps for the reduction of copper oxide to metallic copper have been observed previously and are proposed to arise from varying degrees of interaction of the copper oxide nanoparticles with their supports.[37-39] TPR features at low temperatures indicate smaller CuO particles with a relatively strong interaction with the support, as this interaction can enhance reducibility. The reduction signal at higher temperature is indicative of the formation of larger CuO particles on the surface with weaker support interactions. TPR analysis was also performed for pure t-ZrO_2 and the reduction pattern did not show any signal, indicating that t-ZrO_2 was not reduced up to a temperature of 450 °C.

Comparison of this TPR data with the surface area normalised GVL yields presented in Figure 1b would indicate that, while the reducibility of the CuO content of a catalyst may be an important factor in obtaining a material with high catalytic activity, the vast majority of CuO in the higher loading materials is actually in the form of catalytically inactive spectator species. In the TPR these species are largely reduced below the reaction temperature used in our catalyst testing experiments (200 °C) so this suggests that the large Cu particles that form are not sufficiently active as hydrogenation catalysts to affect the surface area normalised yield.

From the catalytic and analytical results presented so far we conclude that the catalyst prepared with Cu/Zr ratio of 1 was the optimum catalyst composition for LA conversion due to the high surface area of this material. XPS analysis confirmed the presence of CuO, whilst

XRD analysis showed that an amorphous zirconia support and a small particle size of CuO is required for achieving the highest GVL yields. TPR data has shown that CuO particles in all the catalysts with Cu/Zr = 1 and above were reduced under our reaction conditions but yielded broad features (Cu/Zr = 0.75) or no detectable peaks for lower ratios. Hence, only a small amount of Cu in the form of sub-5 nm nanocrystallites is required for an active site to be formed on the catalyst implying that the interaction of these particles with ZrO_2 is also required to achieve activity for the hydrogenation and cyclisation of LA to GVL.

Effect of calcination temperature

Pretreatment of the catalyst precursor, particularly calcination, is a critical part of catalyst preparation which can affect the activity and selectivity of catalysts.[40] In order to study the effect of calcination in this system, Cu-ZrO_2 (Cu/Zr = 1) precipitates prepared with a 6 h aging time following our standard procedure were calcined at different temperatures in static air for 4 h and tested for LA conversion. GVL yield for catalysts prepared from precursors calcined at different temperatures are compared in Figure 4 which also shows the surface area normalised yields. The total surface area of the catalysts was measured by BET (Supplementary information Table S4). The plot in figure 4 shows that the GVL yield for materials calcined at 400 °C is more than twice that found with a catalyst prepared using a 300 °C calcination step. This is despite the observation that the BET surface area obtained for the lower temperature calcination is actually higher, so that the 400 °C calcination temperature is required to obtain the active form of the Cu species required for the reaction.

The total surface area of the catalysts continues to decrease with further increases in calcination temperature, with a corresponding increase in the CuO particle size estimated from XRD peak width (Supplementary Information Table S4). The absolute GVL yield presented in Figure 4, is also found to decrease as the calcination temperature is increased as may be expected from the measured BET surface areas. However, within experimental error, the surface area normalised yields also reduce suggesting that the number/activity of the active copper species is also affected by increasing calcination temperature. The metal surface area was measured by N_2O titration method and the data is provided in Table S6 (supplementary information). The catalysts calcined at 400 and 600 ◦C showed the highest surface area (4.1 m^2g^{-1}). (All these catalysts were reduced prior to N_2O titration therefore the material is not strictly the same material as the catalyst that is used for LA hydrogenation. Therefore, these values can only be taken as estimates).

Figure 5 shows the XRD patterns collected for catalysts obtained with different calcination temperatures. The catalysts from precursors calcined at 300 °C were found to have no reflections corresponding to crystalline phases of zirconia and only small reflections corresponding to CuO (111) at 2θ values of 36°, 39°, and 49° (ICDD-00-041-0254). The CuO(111) reflections became more intense on increasing the calcination temperature up to 600 °C and peaks corresponding to tetragonal zirconia (t-ZrO_2, 2θ = 31.5° (101), 51° (202), 62° (202); ICDD-01-070-8758) begin to appear, indicating an amorphous to crystalline transition takes place. Further increasing the calcination temperature up to 700 °C results in a shift of the main t-ZrO_2 diffraction peak from 2θ = 31.5° to a lower diffraction angle of 2θ = 30.2°. A phase transition from tetragonal to monoclinic ZrO_2 (m-ZrO_2, 2θ = 28° (111), 31° ($\bar{1}$11), 34° (002), 41° (220); ICDD-00-007-0343) was observed with a further increase in calcination temperature from 700 to 800 °C, such phase changes in the ZrO_2 support materials of Cu/ZrO_2 catalysts have previously been observed [41] and simply follow the phase behaviour of ZrO_2 itself [42, 43]. This suggests that the incorporation of copper into ZrO_2 does not have a marked effect on the phase transition temperatures of ZrO_2.

Comparison of the catalytic and XRD data again confirms that the most active catalyst had a relatively small CuO particle size and was supported on amorphous ZrO_2. The formation of the t-ZrO_2 phases had a detrimental effect on activity and synthesis of more crystalline materials with large CuO particle sizes and m-ZrO_2 phases (700 and 800 °C) resulted in a total loss in catalytic activity.

Analysis of the surface elemental concentrations estimated using XPS (Table 1) show that the Cu/Zr ratio for the as-prepared catalysts varies appreciably with calcination temperature. There is also no correlation with Cu concentration and the GVL yields presented in Figure 4, again suggesting that much of the Cu present in these materials is not in a catalytically active form. We note that there is a considerable carbon concentration present along with higher oxygen atom content than would be expected from the metal oxides alone. This may indicate that there is retention of carbonate from the K_2CO_3 used to control pH during the precipitation step of the synthesis.

TPR analysis was also performed on the catalysts calcined at different temperatures and the TPR profiles are shown in Figure 6. The most active catalyst, calcined at 400 °C, was fully reduced below the reaction temperature (200 °C) and showed two well defined reduction signals as discussed previously. The catalysts calcined at 300 and above 400 °C showed

reduction signals above the reaction temperature. This shift to a higher reduction temperature correlates with the increase in CuO particle size for materials calcined at 500 °C or above (Table S4). The increasing breadth of the reduction signal as a function of precursor calcination temperature suggests that bulk-like CuO is formed at the higher calcination temperatures, especially at 800 °C which shows a very broad TPR signal with very little evidence of reduction below 200 °C (Figure 6). Combined with the XRD results, this could suggest that at the highest calcination temperatures there is a segregation of CuO and ZrO_2, as noted by Wang *et al.*[41]. The catalyst calcined at 300 °C, however, does not have reflections in the XRD pattern corresponding to large CuO particle sizes but does exhibit relatively low temperature reduction.

From the discussion of the characterisation of these catalysts so far, it can be seen that the reduction behaviour of well dispersed small CuO clusters with strong interactions with the ZrO_2 support is an important feature of active catalysts. The catalyst that gave the highest GVL yield was that calcined at 400 °C and showed both a high BET surface area and a lower reduction temperature for CuO in the TPR analysis than found for other materials. In the next section we study the effect of precipitate ageing time on catalytic activity for LA hydrogenation.

Effect of the ageing time of precipitates

The Cu-ZrO_2 catalysts prepared with the variation of ageing times between precipitation and calcination (at the optimal 400 °C) were tested for LA conversion and the variation of GVL yield as a function of aging time is presented in Figure 7a. The catalyst prepared with no ageing treatment showed very low activity. An increase in GVL yield was observed with an increase in ageing time up to 6 h. The catalyst aged for 6 h showed the highest yield of GVL. Further increase in the ageing time above 6 h showed a decline in the catalytic activity and the catalyst aged for 24 hours showed the lowest GVL production. The GVL yield normalized using BET surface area is presented in Figure 7b, and follows the same trend.

BET data (Supplementary information Table S5) showed an increase in surface area with an increase in ageing time from 0 to 6 h. A decline in surface area was observed with a further increase in ageing time from 8 to 24 h. Copper surface area was measured using N_2O titration method and the data is presented in Table 2. The catalyst aged for 6 hours showed the highest metal surface area compared with the catalysts aged for longer time intervals. We also measured the surface area before the calcination treatment, this is also shown in table 2, this

shows there was a reduction in Cu surface area upon calcination which is most likely due to sintering.

XRD analysis was performed for the catalysts aged for different time intervals and the XRD patterns are shown in Figure 8. Four reflections corresponding to CuO (111) were observed at 2θ values of 36°, 39°, 49°, and 62° (ICDD-00-041-0254) in the catalyst which did not undergo any ageing treatment. The reflections at 49° and 62° were not observed with an increase in ageing time from 1 h to 16 h but were seen in the catalyst aged for 24 h. The other two diffraction peaks, at 36° and 39°, were present for materials prepared with all aging times. Interestingly, increasing the ageing time from 0 to 6 h (Figure 8) resulted in a broadening of both reflections and the overall pattern suggesting a lower crystallinity compared with the catalysts aged for shorter time intervals. The diffraction peaks at 36° and 39° reappeared when the catalyst was aged for 8 h, and the intensity was found to be similar to that of the catalysts aged for less than 6 h. Further increases in ageing time up to 11 and 16 h showed very different patterns with far less crystallinity. The catalyst aged for 24 h was found to have more distinct peaks inferring a more crystalline material compared with all the other catalysts. This type of relationship between crystallinity and aging time has previously been reported for Cu-ZnO catalysts.[44] Interestingly all the four reflections of CuO at 36°, 39°, 49°, and 62° 2θ (ICDD-00-041-0254) observed in catalyst that was not aged as part of the synthesis procedure reappeared in the catalyst aged for 24 h and both of these materials also showed a similar, low, catalytic activity.

The size of the CuO particles was estimated using the Scherrer equation applied to the (111) diffraction peaks and the data from Figure 8 is provided in Supplementary Information Table S5. As expected from discussion of the diffraction patterns the CuO particle size decreases with an increase in ageing time from 0 to 6 h. Further increases in ageing time from 8 h to 11 h resulted in an amorphous morphology for which the CuO reflections were too indistinct to be used to measure particle size. CuO particle size then increased with longer ageing times up to 24 h. This type of effect has been previously observed in CuMn catalysts prepared by co-precipitation and has been explained as dissolution and reformation of nanoparticles during the aging process which also results in the observed increased particle crystallinity with long ageing times.[45, 46]

Comparing this data with the GVL yields shown in Figure 7a indicates that the less active catalysts showed more intense peaks in the XRD patterns and also had larger CuO

particle sizes. As the CuO phase intensity and the particle size decreased up to an ageing time of 6 h, the activity increases. At longer ageing time, the XRD reflection gradually starts to reappear and larger particles are formed once again. The reformation of the larger nanoparticles also coincides with a decline in the catalytic activity. This is also apparent in the surface area normalised yields of Figure 7b so that the amount of Cu in the required form for activity is also optimised by a 6 h aging of the precipitate.

TPR analysis was also performed on the catalysts prepared with various ageing times and the profiles produced are shown in Figure 9. All catalysts showed two reduction signals at ~155 and ~180 °C. It can be seen that the reduction profiles of the catalysts change with increased ageing. There is both a gradual shift to a lower temperature of the peaks, and a sharpening of the peaks with increased ageing up to 6 h. This is most likely due to dispersal of CuO and the formation of smaller particles on ageing up to this ageing time which can increase the interaction of CuO with the support and in turn result in an enhanced reducibility. The catalyst aged at 6 h showed the highest activity, had the lowest reduction temperature in the TPR and the sharpest reduction signals, indicating the highest reducibility of the materials tested. This trend is reversed on further ageing up to 24 h. The TPR profiles shift to a higher temperature which corresponds to the reformation of the CuO reflections in the XRD.

Extended ageing times appear to have reformed the catalyst into the same state as is found if calcination is used immediately after precipitation. For example, the catalysts that were not aged and those aged for 24 h have very similar XRD patterns, similar particle sizes (10.2 and 12.9 nm respectively), and similar TPR profiles and also gave similar GVL yields of 25.5 % and 22.5 % respectively.

Figure 10 shows the GVL yield as a function of time for the most active catalyst prepared in this study (Cu/Zr = 1, 6 h aging and calcination at 400 °C). The reaction shows no significant induction period and GVL yield increases linearly up to 2 h which was the standard sampling time for earlier discussions of GVL yield. Since GVL was the only product observed and mass balance was 100 % within experimental error this also indicates that the 2 h sample point is a good measure of catalyst activity. After 3 h the reaction has run to completion with 100 % conversion of LA. A linear best fit line to the first 2 h of data gives an estimated rate of 8.90×10^{-5} mol dm^{-3} s^{-1} g_{cat}^{-1} which is comparable with Ru/Sn/C catalyst reported previously.[47]

The most active catalyst was also tested for its activity on reuse cycles. Figure 11 shows that the activity of the catalyst decreases on subsequent uses. MPAES analysis of the reaction

solution showed that leaching from the catalyst is minimal and therefore could not be the cause of the loss of activity. This data is inconsistent with Hengne *et al*[22] who have previously shown a considerable leaching of Cu species from ZrO_2 and Al_2O_3 catalysts when the reactions were carried out in water as well methanol. The XRD pattern of the catalyst after use (Figure S2 Supporting Information) shows the formation of copper metal on the catalyst with a particle size of 38 nm (increased from a CuO particle size of 5.4 nm). So that it appears that Cu particle sintering due to the exposure to harsh reaction conditions is responsible for the deactivation of the catalyst.

Conclusions

The development of an active, and selective catalyst based on inexpensive and abundant metals is highly desirable for the conversion of LA to GVL. We have shown that a Cu-ZrO_2 catalyst prepared by a co-precipitation method can be highly selective for the synthesis of GVL. We have demonstrated that a catalyst prepared with a Cu/Zr ratio of unity has a relatively high surface area and shows around 80 % yield of GVL after 2 h reaction time at 200 °C with an effective rate of 8.90×10^{-5} mol dm^{-3} s^{-1} g_{cat}^{-1}. This suggests that much of the Cu deposited in the co-precipitation process is in an inactive form, either incorporated into the zirconia lattice or present as large particles of CuO. While these large particles can be reduced under our experimental conditions they appear inactive for hydrogenation of LA. This suggests that it should be possible to prepare a material with a much lower Cu loading that would still show higher activity.

Our study of other preparation variables, calcination temperature and aging time confirmed that ageing of the precipitate for 6 h, and calcination of the catalyst at 400 °C resulted in the most active catalyst and highest GVL yield. Lower calcination temperatures did result in higher surface area materials but these were of lower activity.

Acknowledgements

This work was financially supported by the European Union FP7 NMP project NOVACAM (Novel cheap and abundant materials for catalytic biomass conversion, FP7-NMP-2013- EU-Japan-604319). Satoshi Ishikawa is currently a Research Fellow of Japan Society for the Promotion of Science.

References

1. J.-P. Lange, R. Price, P. M. Ayoub, J. Louis, L. Petrus, L. Clarke and H. Gosselink, *Angew. Chem., Int. Ed.*, 2010, **49**, 4479-4483.
2. Y. Roman-Leshkov, C. J. Barrett, Z. Y. Liu and J. A. Dumesic, *Nature*, 2007, **447**, 982-985.
3. E. L. Kunkes, D. A. Simonetti, R. M. West, J. C. Serrano-Ruiz, C. A. Gaertner and J. A. Dumesic, *Science* 2008, **322**, 417-421.
4. G. W. Huber, S. Iborra and A. Corma, *Chem. Rev.* , 2006, **106**, 4044-4098.
5. W. R. H. Wright and R. Palkovits, *ChemSusChem*, 2012, **5**, 1657-1667.
6. M. G. Al-Shaal, W. R. H. Wright and R. Palkovits, *Green Chem.*, 2012, **14**, 1260-1263.
7. A. M. R. Galletti, C. Antonetti, V. De Luise and M. Martinelli, *Green Chem.*, 2012, **14**, 688-694.
8. P. P. Upare, J.-W. Yoon, M. Y. Kim, H.-Y. Kang, D. W. Hwang, Y. K. Hwang, H. H. Kung and J.-S. Chang, *Green Chem.*, 2013, **15**, 2935-2943.
9. S. N. Derle and P. A. Parikh, *Biomass Convers. Biorefin.*, 2014, **4**, 293-299.
10. , CN104230615A, 2014.
11. H. Zhang and T. Zhao, Accessed Copyright (C) 2015 American Chemical Society (ACS). All Rights Reserved.
12. X.-L. Du, Q.-Y. Bi, Y.-M. Liu, Y. Cao, H.-Y. He and K.-N. Fan, *Green Chem.*, 2012, **14**, 935-939.
13. R. V. Christian, Jr., H. D. Brown and R. M. Hixon, *J. Am. Chem. Soc.*, 1947, **69**, 1961-1963.
14. I. T. Horvath, *Green Chem.*, 2008, **10**, 1024-1028.
15. , US2786852, 1957.
16. Z.-p. Yan, L. Lin and S. Liu, *Energy Fuels*, 2009, **23**, 3853-3858.
17. X.-d. Long, Z.-l. Li, G. Gao, C.-g. Xia and F.-w. Li, *Fenzi Cuihua*, 2014, **28**, 384-392.
18. J. Q. Bond, D. M. Alonso, D. Wang, R. M. West and J. A. Dumesic, *Science* 2010, **327**, 1110-1114.
19. H. A. Schuette and R. W. Thomas, *J. Am. Chem. Soc.*, 1930, **52**, 3010-3012.
20. L. E. Manzer, *Appl. Catal., A*, 2004, **272**, 249-256.
21. , US6054611A, 2000.
22. A. M. Hengne and C. V. Rode, *Green Chem.*, 2012, **14**, 1064-1072.
23. R. A. Bourne, J. G. Stevens, J. Ke and M. Poliakoff, *Chem. Commun.* , 2007, 4632-4634.
24. S. Cao, J. R. Monnier, C. T. Williams, W. Diao and J. R. Regalbuto, *J. Catal.*, 2015, **326**, 69-81.
25. W. Luo, U. Deka, A. M. Beale, E. R. H. van Eck, P. C. A. Bruijnincx and B. M. Weckhuysen, *J. Catal.*, 2013, **301**, 175-186.
26. , WO2015026234A1, 2015.
27. Y. Kuwahara, Y. Magatani and H. Yamashita, *Catal. Today*, 2015, Ahead of Print.
28. A. M. Ruppert, J. Grams, M. Jedrzejczyk, J. Matras-Michalska, N. Keller, K. Ostojska and P. Sautet, *ChemSusChem*, 2015, 1657-1667.
29. V. Swarna Jaya, M. Sudhakar, S. Naveen Kumar and A. Venugopal, *RSC Adv.*, 2015, **5**, 9044-9049.
30. P. P. Upare, M.-G. Jeong, Y. K. Hwang, D. H. Kim, Y. D. Kim, D. W. Hwang, U. H. Lee and J.-S. Chang, *Appl. Catal., A*, 2015, **491**, 127-135.
31. J. Tan, J. Cui, T. Deng, X. Cui, G. Ding, Y. Zhu and Y. Li, *ChemCatChem*, 2015, **7**, 508-512.
32. P. Balla, V. Perupogu, P. K. Vanama and V. c. Komandur, *J. Chem. Technol. Biotechnol.*, 2015, Ahead of Print.
33. S. Y. Fu, Y. Z. Li, W. Chu, C. Li and D. G. Tong, *Catal. Sci. Technol.*, 2015, **5**, 1638-1649.
34. K. Yan, J. Liao, X. Wu and X. Xie, *RSC Adv.*, 2013, **3**, 3853-3856.
35. J. Yuan, S.-S. Li, L. Yu, Y.-M. Liu, Y. Cao, H.-Y. He and K.-N. Fan, *Energy Environ. Sci.*, 2013, **6**, 3308-3313.
36. E. F. Mai, M. A. Machado, T. E. Davies, J. A. Lopez-Sanchez and V. Teixeira da Silva, *Green Chem.*, 2014, **16**, 4092-4097.
37. S. Sitthisa, W. An and D. E. Resasco, *J. Catal.*, 2011, **284**, 90-101.
38. J. Sloczynski, R. Grabowski, A. Kozlowska, P. K. Olszewski and J. Stoch, *Phys. Chem. Chem. Phys.*, 2003, **5**, 4631-4640.

39. M. Shimokawabe, H. Asakawa and N. Takezawa, *Appl. Catal.*, 1990, **59**, 45-58.
40. B. Solsona, G. J. Hutchings, T. Garcia and S. H. Taylor, *New J. Chem.*, 2004, **28**, 708-711.
41. L.-C. Wang, Q. Liu, M. Chen, Y.-M. Liu, Y. Cao, H.-Y. He and K.-N. Fan, *J. Phys. Chem. C*, 2007, **111**, 16549-16557.
42. S. Xie, E. Iglesia and A. T. Bell, *Chem. Mater.*, 2000, **12**, 2442-2447.
43. C. Li and M. Li, *J. Raman Spectrosc.*, 2002, **33**, 301-308.
44. A. A. Mirzaei, H. R. Shaterian, S. H. Taylor and G. J. Hutchings, *Catal. Lett.*, 2003, **87**, 103-108.
45. G. J. Hutchings, A. A. Mirzaei, R. W. Joyner, M. R. H. Siddiqui and S. H. Taylor, *Appl. Catal., A*, 1998, **166**, 143-152.
46. D. M. Whittle, A. A. Mirzaei, J. S. J. Hargreaves, R. W. Joyner, C. J. Kiely, S. H. Taylor and G. J. Hutchings, *Phys. Chem. Chem. Phys.*, 2002, **4**, 5915-5920.
47. S. G. Wettstein, J. Q. Bond, D. M. Alonso, H. N. Pham, A. K. Datye and J. A. Dumesic, *Appl. Catal., B*, 2012, **117-118**, 321-329.

Figures and Tables

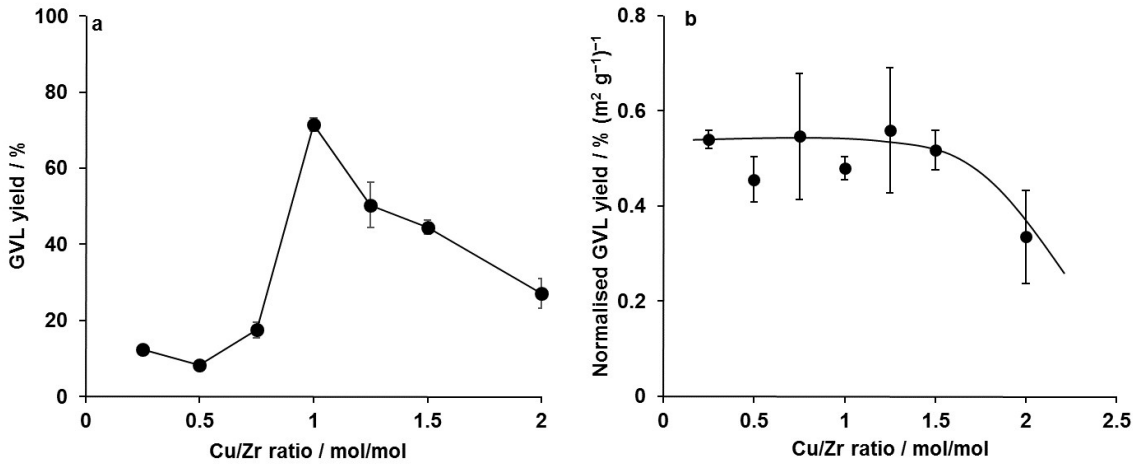

Figure 1. Effect of the variation of Cu/Zr molar ratio on GVL yield from LA hydrogenation. *Key*: *a*. GVL yield; *b*. GVL yield normalised by BET surface area. *Reaction conditions*: 200 °C, H_2 35 barg, 2 h, LA 5 wt.% in water, catalyst 0.05 g. The error bars shown are based on triplicate experiments.

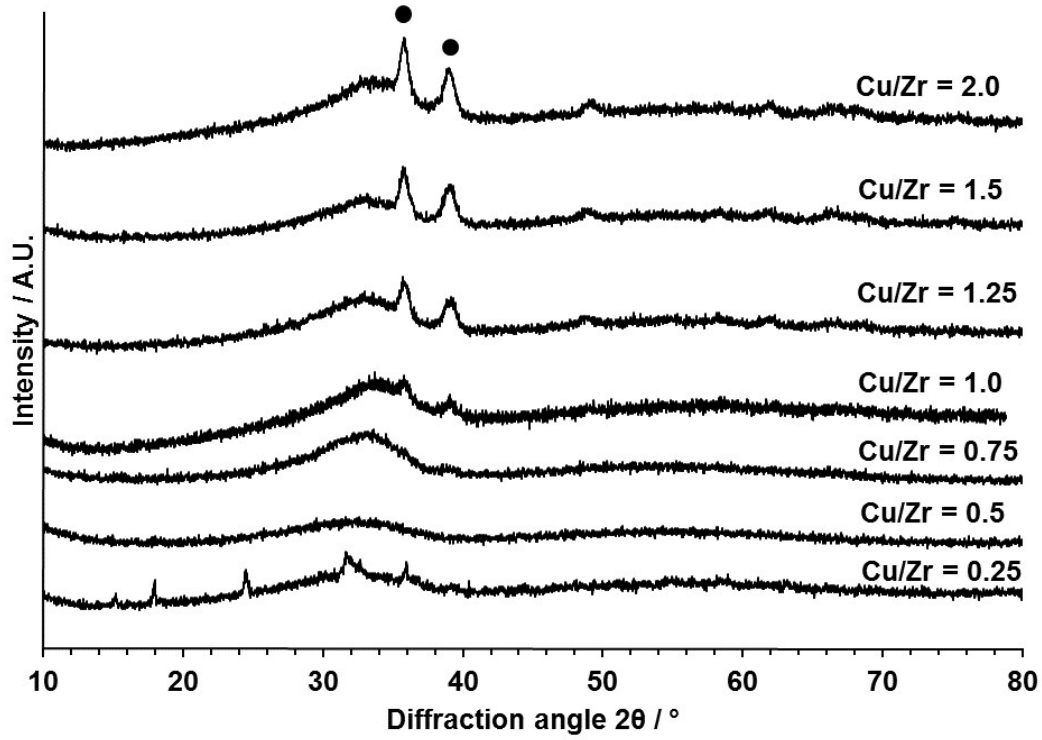

Figure 2. XRD pattern for the catalysts prepared with various Cu/Zr molar ratios. ● CuO

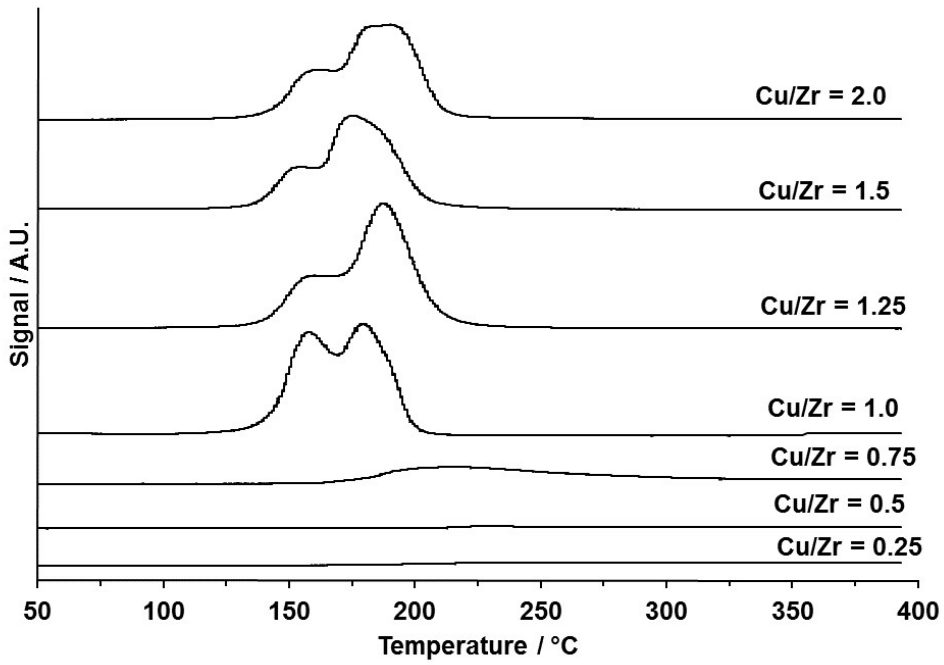

Figure 3. TPR profiles of the catalysts prepared with various Cu/Zr ratio

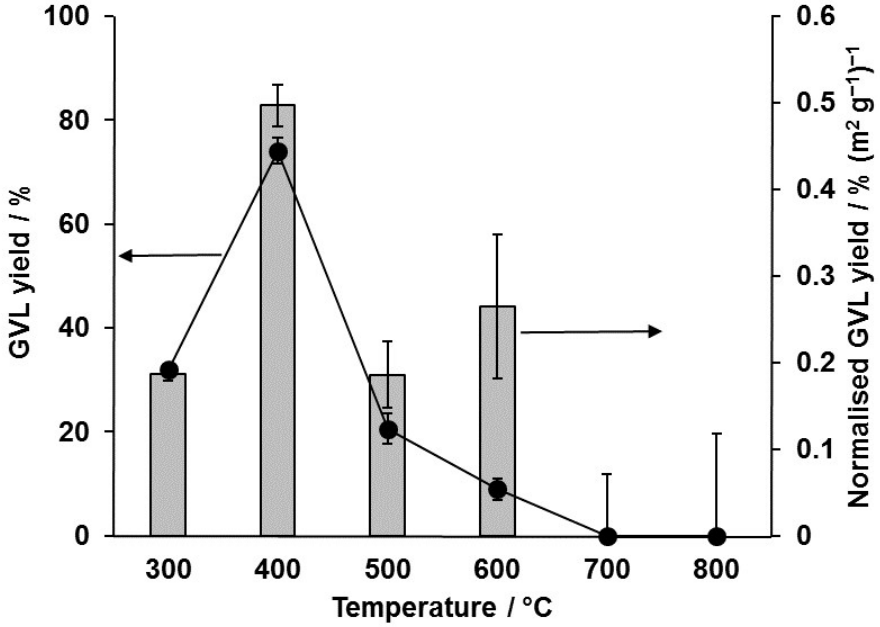

Figure 4. Effect of the variation of calcination temperature of Cu-ZrO_2 catalysts on GVL yield. *Key*: Line graph: GVL yield; Manhattan plot: GVL yield normalised by BET surface area. *Reaction conditions*: 200 °C, H_2 35 bar, 2 h, LA 5 wt.% in water, catalyst 0.05 g.

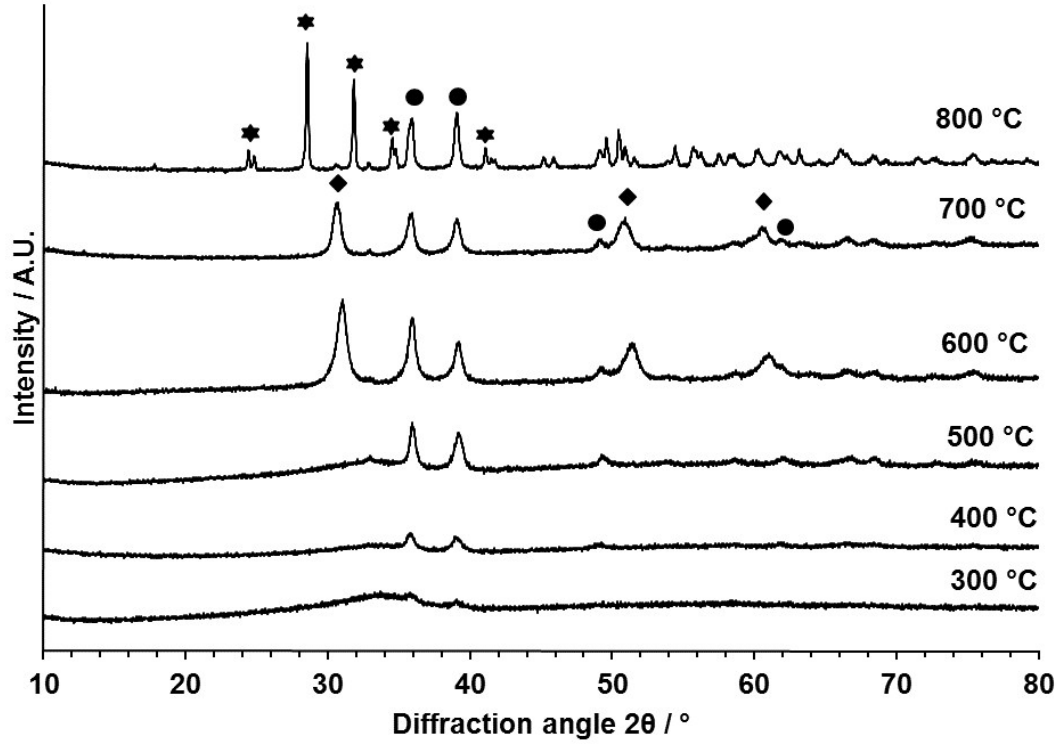

Figure 5. XRD patterns of Cu-ZrO_2 catalysts (Cu/Zr = 1) calcined at different temperatures. *Key*: ● CuO; ♦ t-ZrO_2; ★ m-ZrO_2,

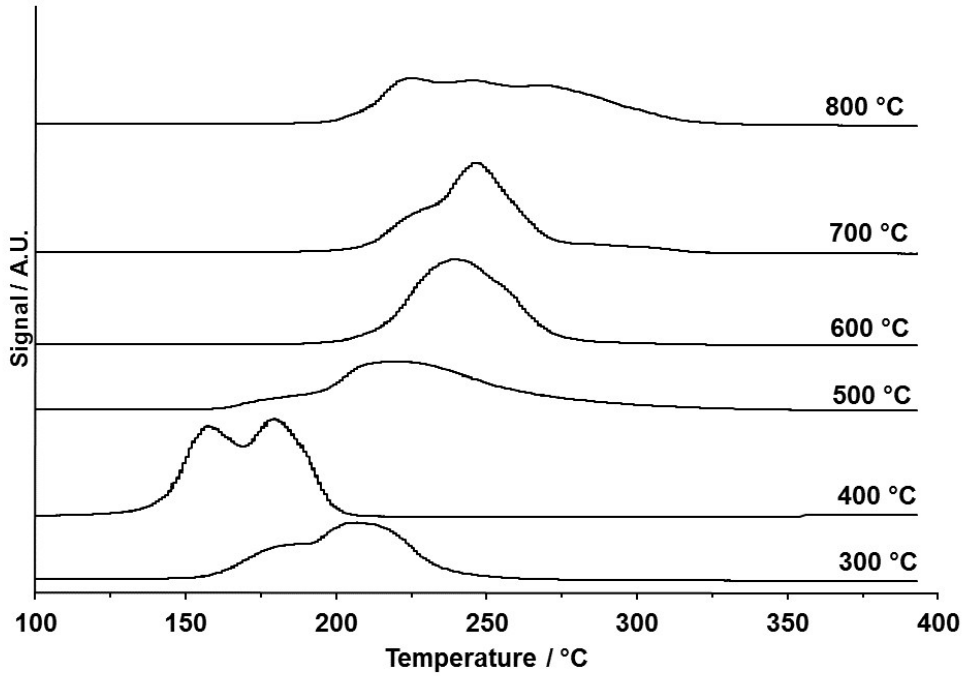

Figure 6. TPR profiles of the catalysts prepared with the variation of calcination temperatures.

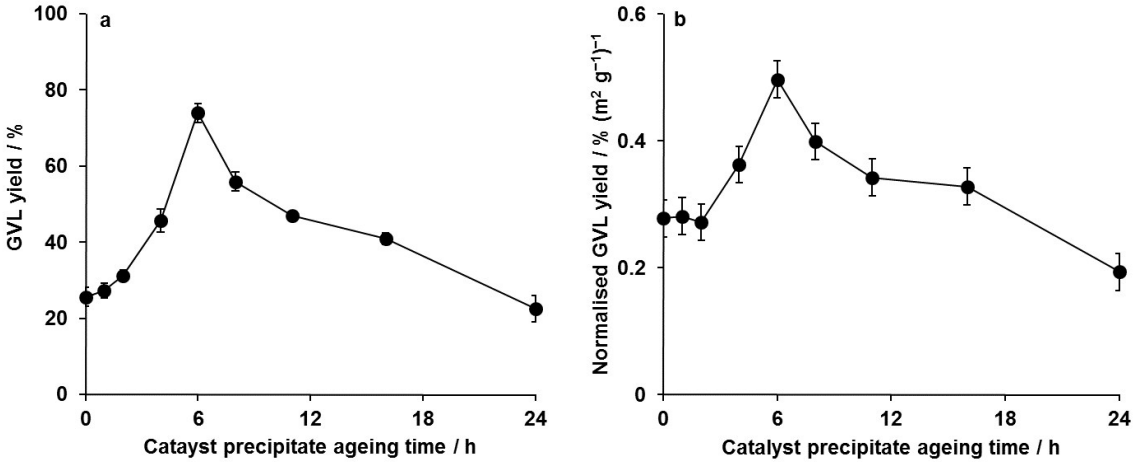

Figure 7. Catalytic activity of Cu-ZrO_2 catalysts prepared with different ageing times *Key*: a. GVL yield; b. GVL yield normalised by BET surface area. *Reaction conditions*: 200 °C, H_2 35 bar, 2 h, LA 5 wt.% in water, catalyst 0.05 g

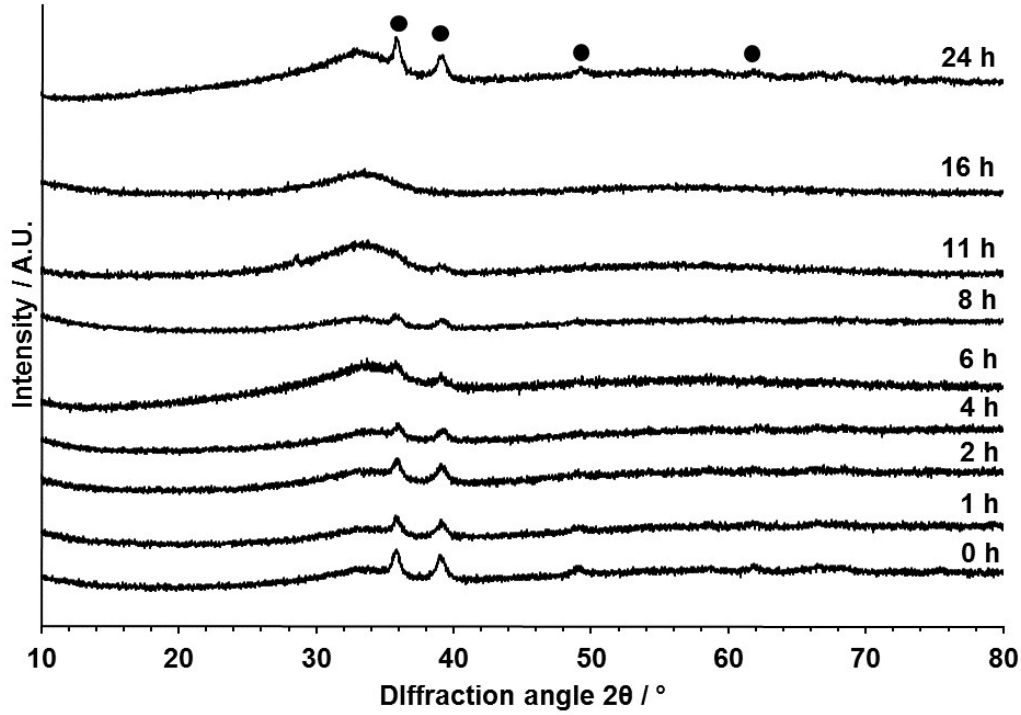

Figure 8. XRD patterns of catalysts prepared with different ageing times. *Key*: ● CuO

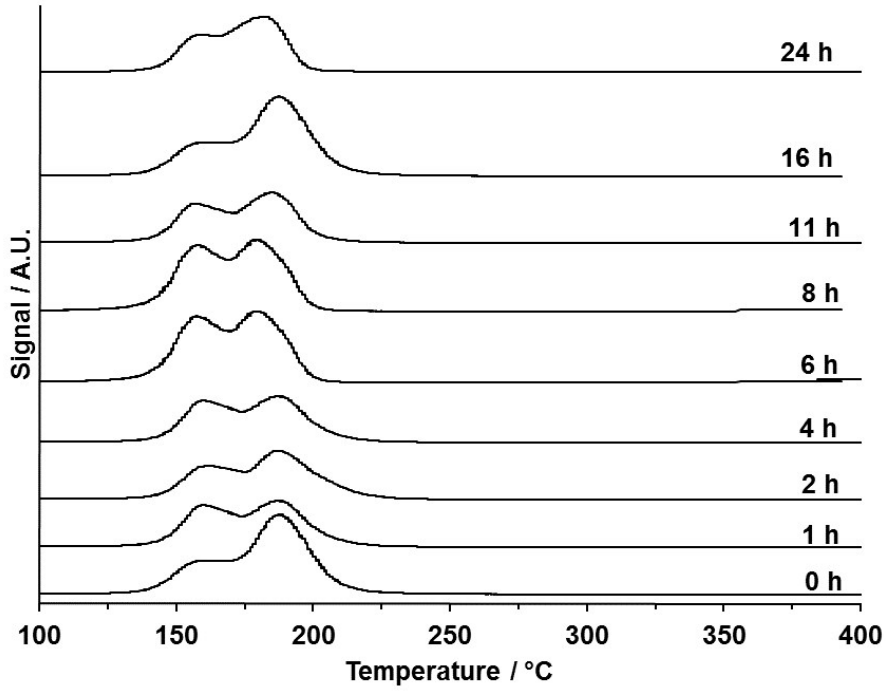

Figure 9. TPR profile of catalysts prepared with different ageing times.

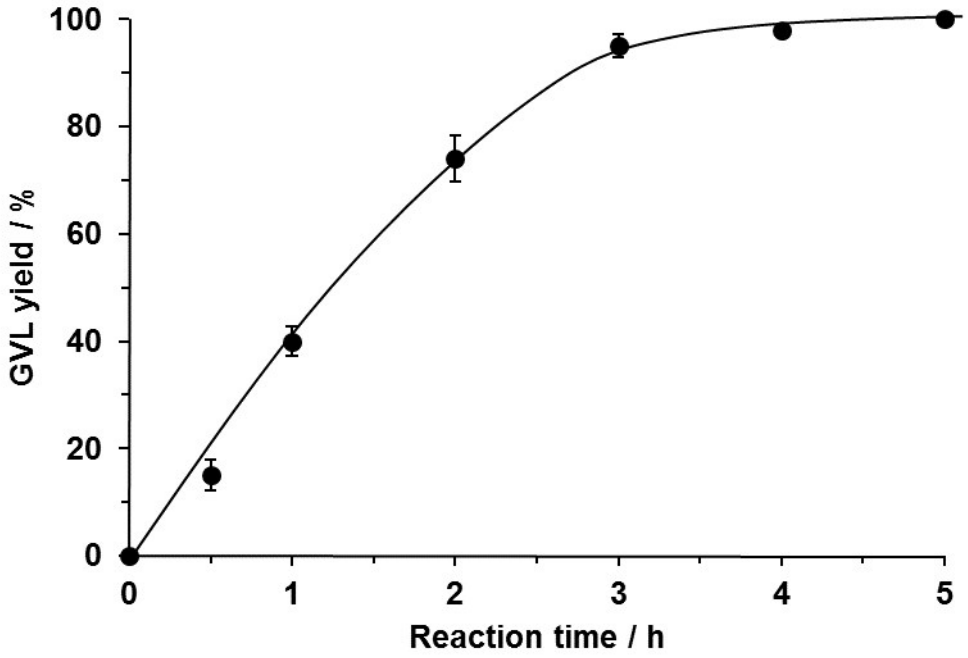

Figure *10*. Time-on-line data for the Cu-ZrO_2 catalyst prepared with Cu/Zr = 1, with a precipitate aged for 6 h, and calcined at 400 °C. *Reaction conditions*: 200 °C, 35 bar H_2, 5 wt.% LA/H_2O, 0.05 g catalyst.

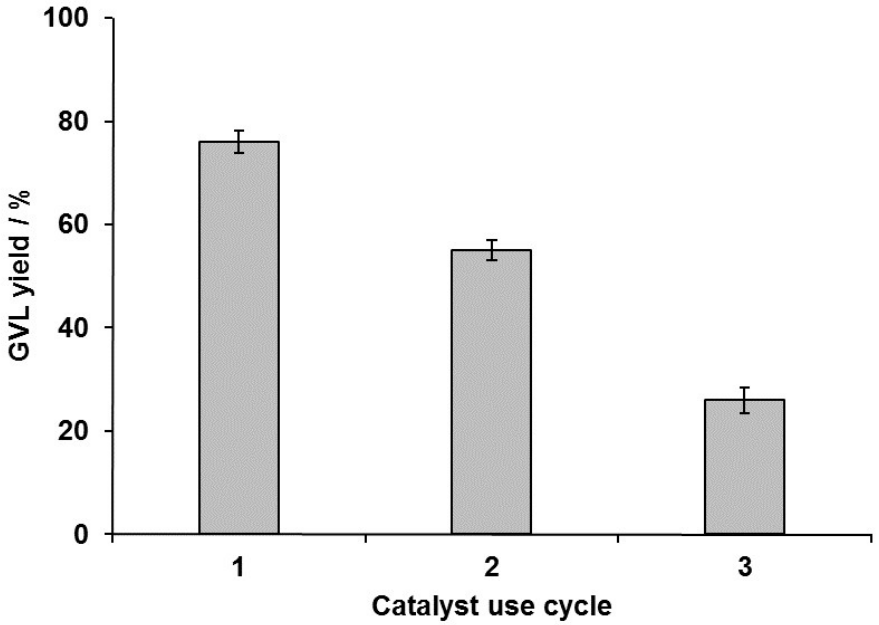

Figure *11*. Cu-ZrO_2 activity after subsequent uses. *Reaction conditions*: 200 °C, 35 bar H_2, 2 h, 5 wt.% LA/H_2O, catalyst 0.05 g.

Table *1*. XPS derived molar composition (at.%) for increasing calcination temperature.

	Surface Elemental Concentration / at.%	Ratio

Temp. (°C)	Cu 2p	O 1s	C 1s	Zr 3d	Cu/Zr
Uncalcined	5.74	26.28	62.96	5.01	1.15
300	4.94	15.56	77.33	2.18	2.27
400	3.92	22.75	68.29	5.03	0.78
500	8.35	25.23	61.07	5.36	1.56
600	8.39	28.05	56.94	6.62	1.27
700	9.62	34.98	45.71	9.69	0.99
800	18.29	46.89	26.23	8.59	2.12

Table *2*. Cu surface area as determined by N_2O titration for Cu-ZrO_2 catalysts prepared with different precipitate ageing times.

Cu-ZrO_2 precipitate ageing time / h	Cu surface area / $m^2\ g^{-1}$
0	2.6
6*	6.0
6	4.1
8	3.4
16	2.1
24	1.5

*Cu surface area measured before calcination at 400 °C

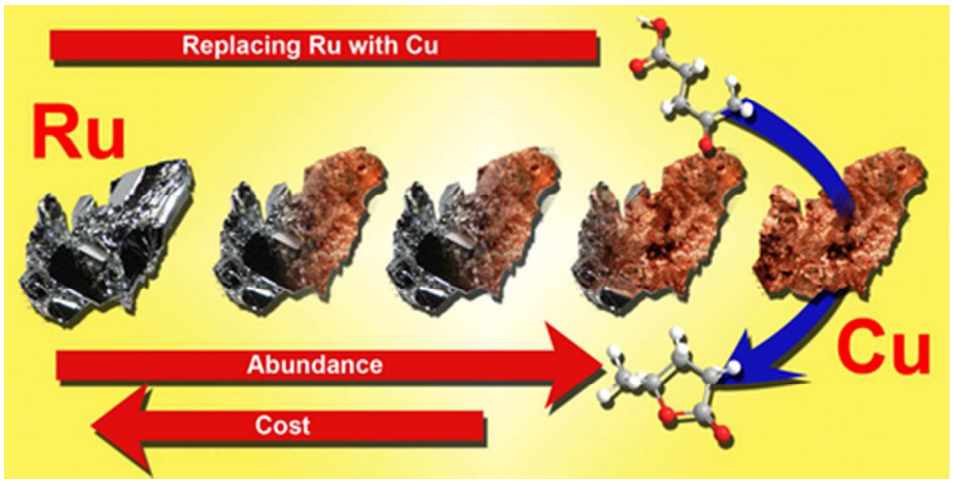

39x19mm (300 x 300 DPI)